INFLUENCE OF ELASTIC DEFORMATION ON THE PRESSURE DISTRIBUTION IN TEXTURED SURFACES

MANEL RODRÍGUEZ RIPOLL*, VICTOR G. MARIAN**, BOJAN PODGORNIK*, JOŽE VIŽINTIN*
*Centre for Tribology and Technical Diagnostics, University of Ljubljana, Slovenia
** Laboratory for Machine Elements and Tribology, University Politehnica of Bucharest, Romania
Corresponding author: manel.rodriguez@ctd.uni-lj.si

Texturing of functional surfaces has gained attention in the past year as a technique for reducing friction in engineering applications. However, the relying mechanism is not yet completely understood. It has been stated that the dimples work as hydrodynamic bearings and a net pressure build up occurs as the contact area slides over a dimple. In this paper, the contribution of the elastic deformation that the borders of the dimples undergo during sliding contact is investigated using the Reynolds equation. The results show that changes of the dimple morphology in the micrometer range substantially affect the pressure distribution.

Key words: Hydrodynamic Lubrication, Reynolds Equation, Textured Surface

The use of textured surfaces as a way for decreasing friction in lubricated contacts has steadily gain attention in the past years [1]. The reason for the decrease in friction of textured surfaces in the hydrodynamic regime has been analysed by many authors using different computational fluid dynamics tools. The most common approach is based on modelling a flat surface sliding over a single dimple using the Reynolds equation [e.g. 2]. The results always follow the same trend independently of the dimple geometry. For a given film thickness, there is an antisymmetric pressure distribution, characterized by a pressure decrease at the diverging region of the dimple followed by an increase in the converging zone. The pressure decrease is typically attributed to cavitation phenomena and is conveniently treated by using the (half/full) Sommerfeld or Reynolds boundary conditions or eventually by using a more realistic cavitation algorithm [3]. In all cases, the pressure rise at the convergence zone of the dimple is the responsible of the pressure build up and, consequently, of the reduction in friction. An analogous result can be obtained using the Navier-Stokes (NS) equation. For low Reynold numbers the predictions of both equations are similar. For large Reynolds numbers, NS predicts a pressure distribution with a net pressure rise as a consequence of convective forces [4,5].

In the present work, textured surfaces under hydrodynamic lubrication are analysed using the Reynolds equation. The contribution of the dimple morphology and the flow conditions to friction reduction are analysed with special attention to geometrical changes caused by elastic deformation during contact. The results of finite element simulations show that during sliding contact, the magnitude of the elastic deformation of a textured surface is comparable to the film thickness. This effect causes that the surface beneath the contact area briefly descends under normal loading and recovers its original position after unloading, when the sliding contact area has moved away. This oscillatory movement in the vicinity of the dimple may cause the dimple to behave as a micropump and contribute to friction reduction. A similar

squeeze effect was proposed by other authors [6-8] as a mechanism for friction reduction in textured surfaces.

FINITE ELEMENT SIMULATIONS

Finite element simulations were performed using the code Z-Set/ZéBuLoN [9]. The 2D plane strain model represents a cylinder and a flat surface. The surface contains dimples with a diameter of 100 μm and a depth of 10 μm. The distance between dimples is set to 200 μm. The simulations were performed under a constant load, with values ranging from 20 to 90 N. The selected parameters represent typical experimental conditions. For further details concerning the finite element simulations, the reader is referred to [10].

Under dry contact conditions, the contact area slides over a single dimple at a time. The finite element simulations predict an elastic deformation – or elasto-plastic depending on the load – as a consequence of the Hertzian contact. The magnitude of the deflection is rather small, of the order of 0.5 to 1.0 μm. However, this range of values has the same order of magnitude as typical film thickness in hydrodynamic lubricated contacts. This means that, during wet contact, the surface area below the sliding cylinder may deform, as schematically shown in Figure 1. The cylinder slides over the plane from right to left. Firstly, the right edge of the dimple deforms vertically (Fig. 1a). Afterwards, the contact area moves and is placed over the dimple. In this case, both edges of the dimple are compressed (Fig. 1b). Then the right edge is released while the left is kept compressed (Fig. 1c) before finally being released in order to return to the original configuration.

During this process, the dimple morphology is changed and the film thickness between the contact surfaces will be different at the contact position. In what follows, this deformation will be imposed when applying the Reynolds equation, in order to study its consequences in the pressure distribution during hydrodynamic sliding contact.

a)   b)   c)
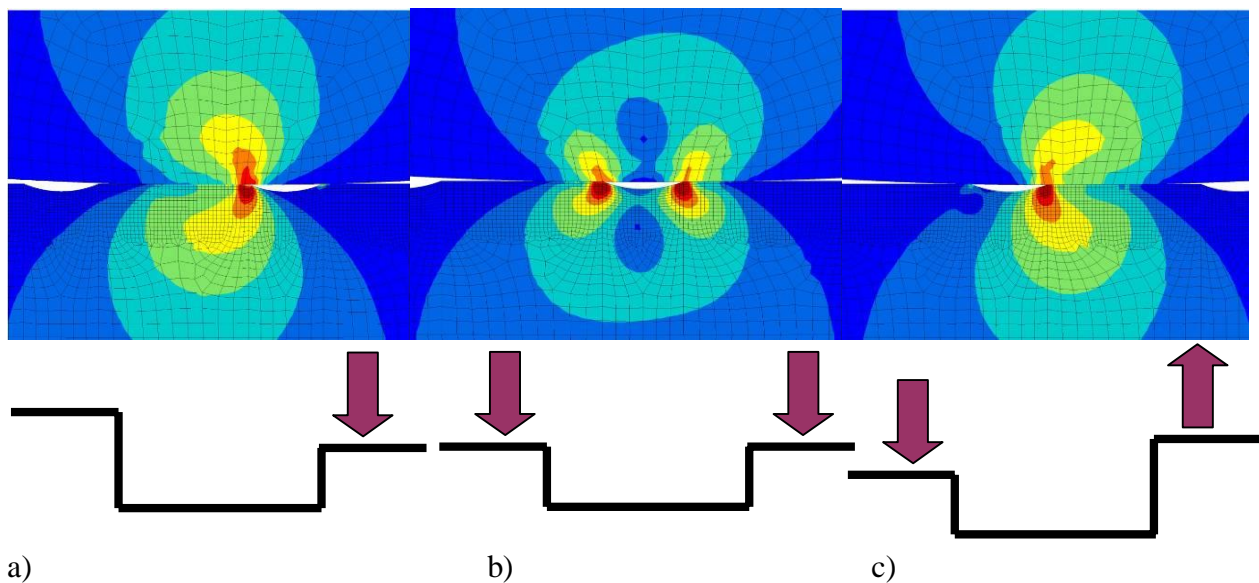
Figure 1. Finite Element simulation showing a cylinder sliding over a dimple. Below, it is shown an schematic representation of the vertical displacement undergone by the textured surface in the vicinity of the dimple.

30

HYDRODYNAMIC SIMULATIONS

Reynolds Equation

The pressure distribution caused by a dimple is calculated using the Reynolds equation. The variables used in the equations are illustrated in Figure 2.
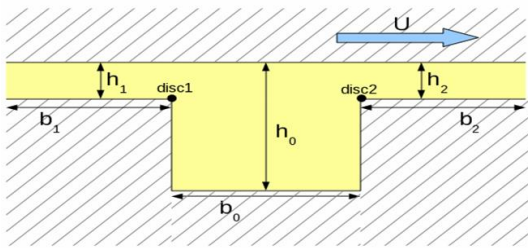
Figure 2. Sketch of a dimple showing the most relevant variables.

Since the borders of the dimple are allowed to oscillate, the Reynolds equation includes the squeeze term in its right-hand side and has the following form:

$$\frac{\partial}{\partial x}\left(h_i^3 \frac{\partial p}{\partial x}\right) + \frac{\partial}{\partial y}\left(h_i^3 \frac{\partial p}{\partial y}\right) = 12\eta \frac{\partial h_i}{\partial t} \qquad (1)$$

where p denotes the pressure, η is the viscosity of the lubricant and h_i is the film thickness in the i section of the dimple.

At the deep part of the dimple, the film thickness h_0 is constant and equation (1) becomes the Laplace equation

$$\frac{\partial^2 p}{\partial x^2} + \frac{\partial^2 p}{\partial y^2} = 0 \qquad (2)$$

At the edges of the dimple, the film thickness is allowed to oscillate and h_i takes the following values:

$$h_1 = h_{1ref} + \Delta h \cos(\omega t) \qquad (3)$$

and

$$h_2 = h_{2ref} + \Delta h \sin(\omega t) \qquad (4)$$

In both equations, h_{1ref} and h_{2ref} are the central values of the oscillation and Δh is the amplitude. The film thickness oscillates with an angular frequency ω, which is given as 2π divided by the period of the oscillation

$$\omega = \frac{2\pi U}{b_1 + b_0 + b_2} \qquad (5)$$

where U is the sliding velocity and the term $b_1 + b_0 + b_2$ is the length of the dimple plus its edges.

The system is completely defined by applying the flow continuity equation at the discontinuity points, indicated as disc1 and disc2 (Fig. 2).

$$q_x = -\frac{h_i^3}{12\eta}\frac{\partial p}{\partial x} + U\frac{h_i}{2} \qquad (6)$$

As boundary condition, the pressure p is set to zero at $x = 0$ and $x = b_1 + b_0 + b_2$.

RESULTS

Reference Case

The Reynolds equation (1) and the flow continuity equation (6) are transformed into a system of algebraic equations using finite differences. This system of algebraic equations is solved using the Gauss-Seidel algorithm and implemented into a stand alone Fortran code.

The parameters for the dimple dimensions and the tribological conditions are selected to represent values typically found in experiments (Table 1).

Table 1. Simulation parameters for the reference case.

Parameters for the reference case	
Dimple Morphology	
b_0	50 μm
b_1	100 μm
b_2	100 μm
h_{1ref}	10 μm
h_{2ref}	10 μm
h_0	15 μm
Δh	0.1 μm
Tribological Conditions	
U	0.5 m/s
η	46.10^{-3} Pas

Firstly, as a reference, the pressure distribution for an undeformed dimple is calculated, so that Δh is set to 0 (Fig. 3). This pressure profile corresponds to the classical pressure distribution characterized by a pressure decrease in the diverging zone of the dimple and by a pressure rise in the converging zone. As mentioned, negative pressures in the diverging zone are typically attributed to lubricant cavitation or starvation.

The results of the simulations are presented for four different values of an oscillation cycle, namely $\omega t = 90$, 180, 270 and 360 (Fig. 4). The position of the dimple is indicated by the dashed lines.

For $\omega t = 90$, the left edge of the dimple starts moving down, while the other edge is at the highest position. This describes the situation where the contact area is in the first edge of the dimple. Under these conditions, the pressure distribution shows a pressure profile, charac-terized by a smaller minimum pressure in the diverging zone and a higher maximum pressure in the converging zone (Fig. 4a). Additionally, the pressure distribution in the diverging zone has a smaller decreasing rate, when compared with the undeformed case. Both characteristics of the pressure profile lead to a net pressure rise when the pressure distribution is integrated over the whole dimple length.
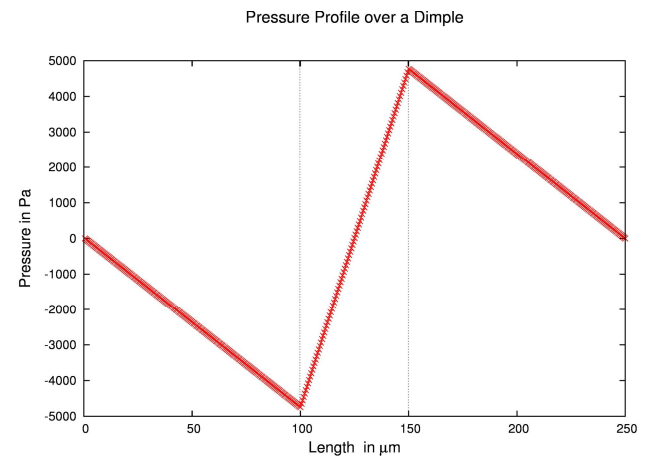
Figure 3. Pressure distributions over an undeformed dimple.

For $\omega t = 180$, the first edge of the dimple is at its minimum position, while the second edge is at the intermediate position. This morphology builds up a pressure distribution similar to $\omega t = 90$, characterized by a region of negative pressure values over the first edge of the dimple followed by a pressure rise (Fig. 4b). At this point of the oscillation, the maximum pressure value of the whole cycle is achieved.

After $\omega t = 180$, the situation of the edges of the dimple changes and the second edge of the dimple starts being in a higher position than the first edge. For instance, when $\omega t = 270$, the first edge of the dimple is in the intermediate position, while the second is at its minimum. This situation is the opposite of the situation found for $\omega t = 180$ and for this reason, the pressure distribution shows a profile antisymmetric to the former one (Fig. 4c). In this case, the pressure build up at the second edge of the dimple is smaller, while larger negative pressure values are found at the first edge of the dimple.

Finally, for $\omega t = 360$, the first edge of the dimple is at its maximum position and the second edge is at the intermediate position. The pressure distribution is antisymmetric to the one found at $\omega t = 90$ (Fig. 4d). Obviously, the results for $\omega t = 0$ are identical to the ones obtained for $\omega t = 360$.
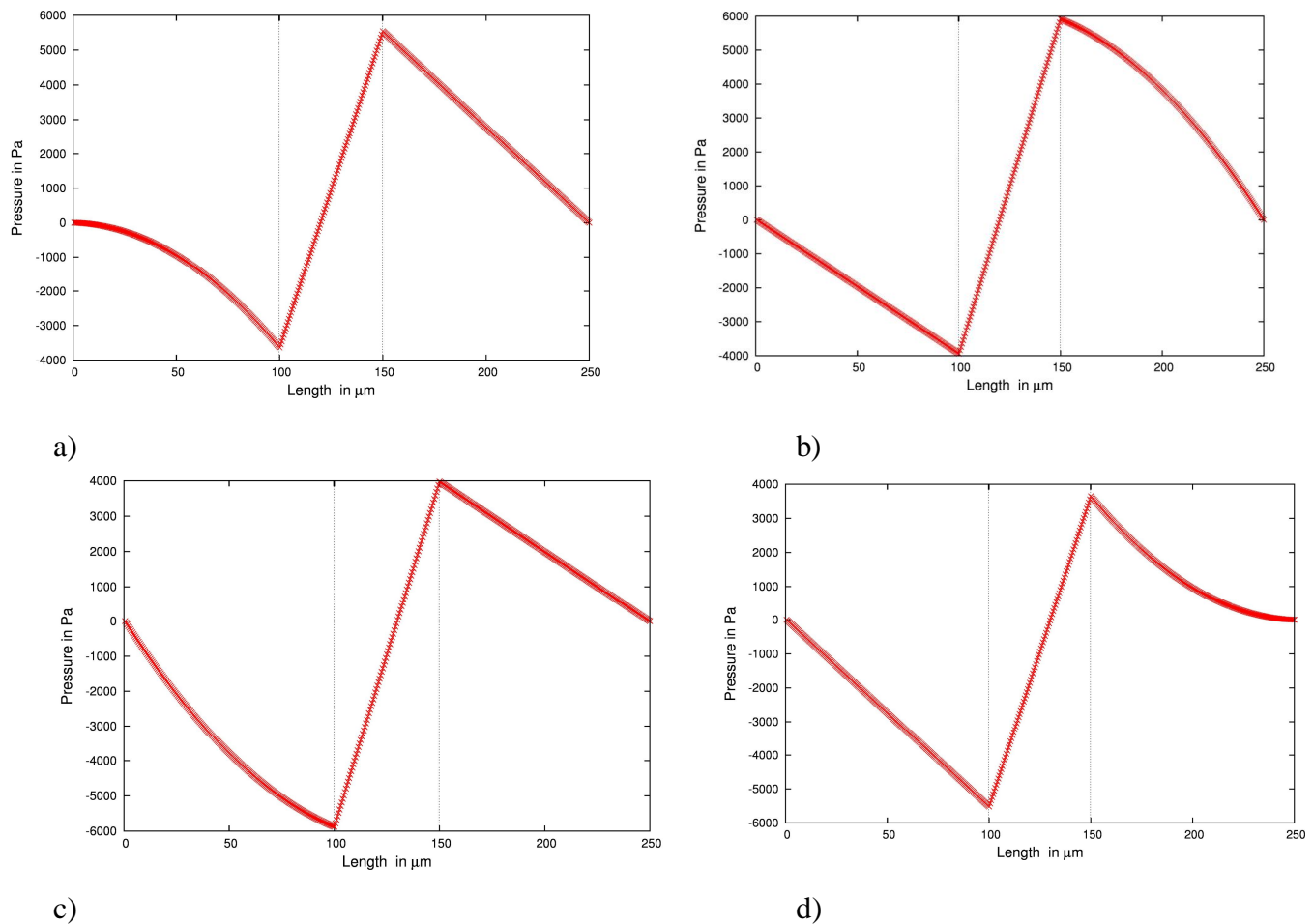
a)

b)

c)

d)

Figure 4. Pressure distributions over a dimple during sliding hydrodynamic contact for a) ωt = 90,
b) ωt = 180,
c) ωt = 270 and d) ωt = 36

Influence of the Oscillation Amplitude

The influence of the oscillation amplitude in the pressure distribution is studied for four different values of *Δh*, namely 0.1, 0.2, 0.3 and 0.5 μm. The results are shown in Figure 5. The two curves presented in each graphic correspond to the situation where *ωt* = 90 and 180. As mentioned in the previous section, the results for *ωt* = 270 and 360 are antisymmetric to the former ones.

For our reference value (*Δh* = 0.1 μm) it can be observed in both curves that the pressure distribution has negative values in the diverging zone and larger positive values in the converging zone (Fig. 5a). Since most of the area below the pressure profile corresponds to positive values, a net pressure build up is obtained.

33

a)

b)

c)

d)
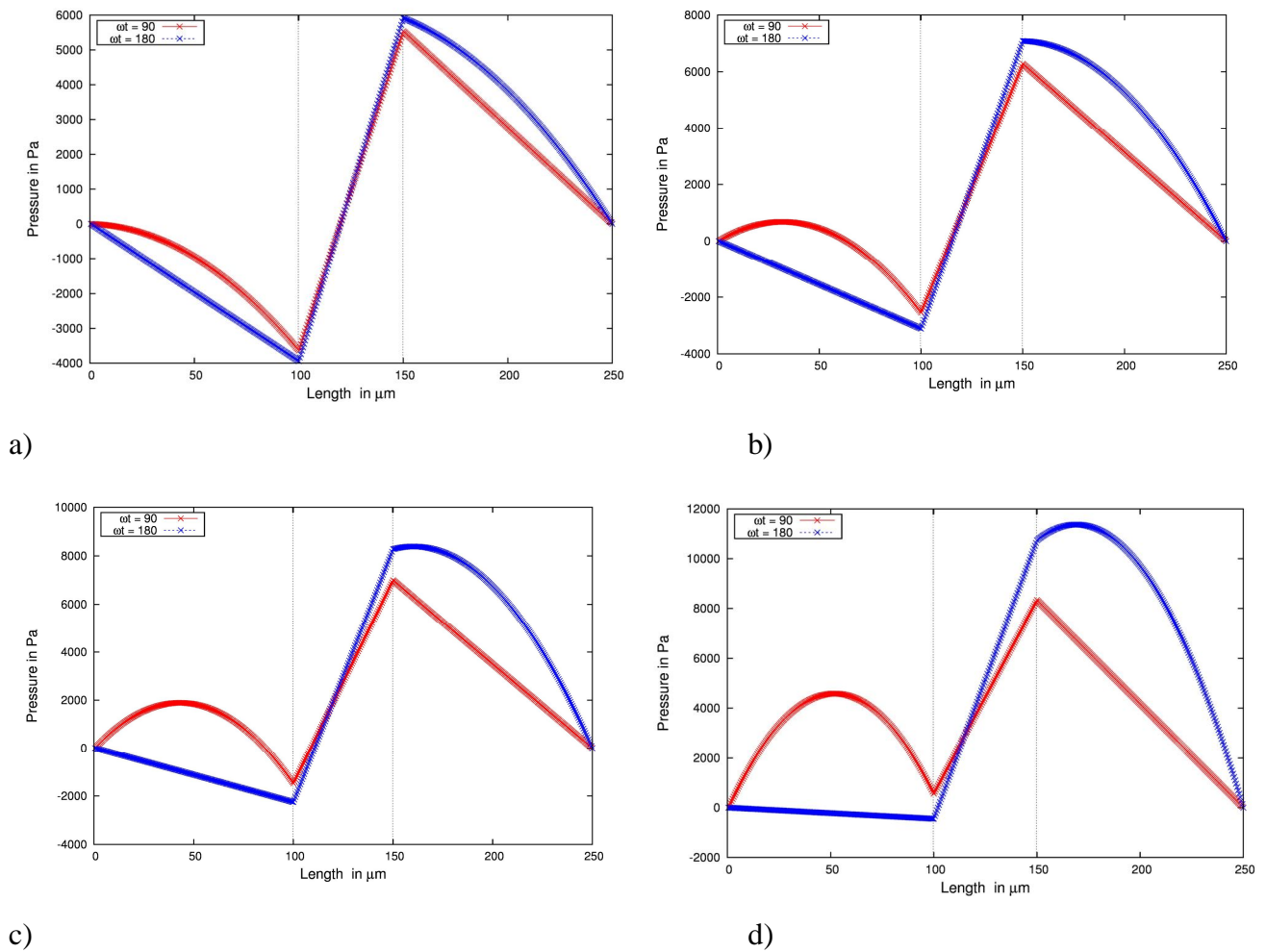
Figure 5. Pressure distributions over a dimple during sliding hydrodynamic contact for and amplitude oscillation of
Δh = 0.1, 0.2, 0.3 and 0.5 μm (ωt = 90 and ωt = 180)

As the amplitude of the oscillation increases, the regions with negative pressure values become smaller (Fig. 5b, 5c). For instance, for *Δh* = 0.5 μm (Fig. 5d), no negative values are present in the pressure distribution for *ωt* = 90 and they are very small for *ωt* = 180. For increasing value of the oscillation amplitude, the maximum pressure values achieved become also larger.

According to these results, a larger oscillation as a consequence of elastic deformation is beneficial for obtaining a larger pressure build up and consequently, a larger friction reduction.

Influence of the Dimple Border Length

This section studies the influence of the dimple border length on the pressure distribution. It is expected that the length of the dimple border, which is deflected in vertical direction, increases for larger contact pressures. In what follows, we study the pressure distribution for the following dimple border lengths: $b_1 = b_2 = 20$, 50, 100 and 200 µm (Fig. 6 a-d).

Firstly, it is observed that the difference between the pressure profiles obtained at different values of ωt during an oscillation cycle increase. For small dimple border lengths, $b_1 = b_2 = 20$ µm (Fig. 6a), the pressure profiles almost overlap each other, while for $b_1 = b_2 = 200$ µm (Fig. 6d), the difference between pressure profiles is evident for $\omega t = 90$ and 180. Further, the pressure values increase and decrease linearly for shorter lengths, as they do in the undeformed case (Fig. 3), which is not valid for longer lengths.

Finally, when the length of the dimple border which is in oscillation increases, higher pressure values are obtained, which means a higher friction reduction.

a)

b)

c)

d)
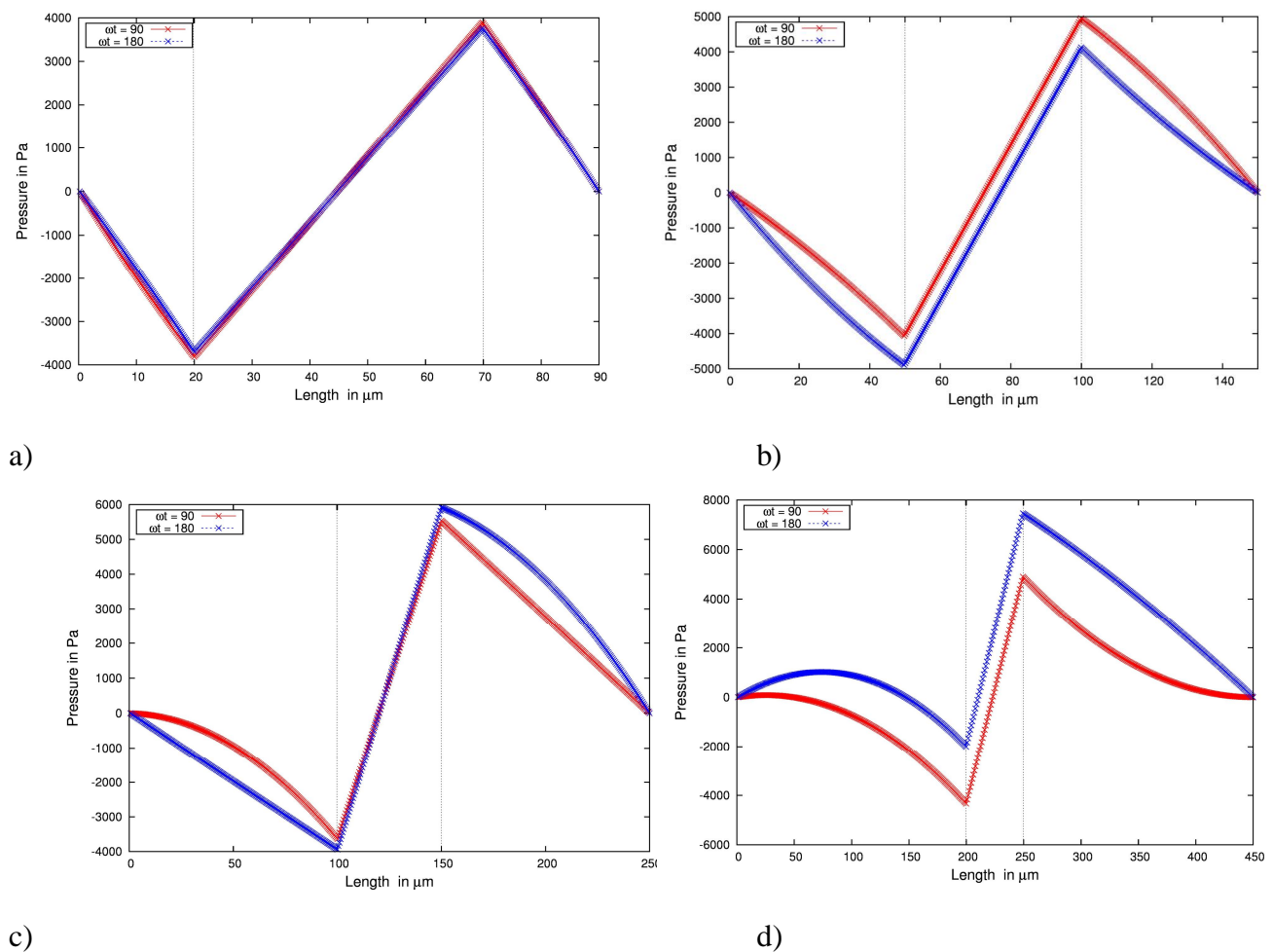
Figure 6. Pressure distributions over a dimple during sliding hydrodynamic contact for a dimple border length oscillation of $b_1 = b_2 = 20$, 50, 100 and 200 µm ($\omega t = 90$ and $\omega t = 180$).

CONCLUSIONS

Finite Element Simulations suggested that for typical texturing parameters, the contact area of the dimples undergoes elastic deformation.

When small vertical oscillations of the dimple borders in the order of (sub)microns are allowed in hydrodynamic simulations, it is observed that they have a strong influence in the pressure distribution profile. This impact increases for larger oscillation amplitudes and for larger dimple border lengths.

REFERENCES

[1] Etsion, I. State of the Art in Laser Surface Texturing, J. Trib. Trans. ASME, 127 (2005), 248-253.

[2] Etsion, I. and Haperin, A Laser Surface Textured Hydrostatic Mechanical Seal, Sealing Tech. (2003) 6-10.

[3] Sahlin, F. et al., A Cavitation Algorithm for Arbitrary Lubricant Compressibility, Trib. Int. 40 (2007) 1294-1300.

[4] Arghir, M. et al., Theoretical Analysis of the Incompressible Laminar Flow in a Macro-Roughness Cell, J. Trib. 125 (2003) 309-318.

[5] Sahlin, F. et al., Two-Dimensional CFD-Analysis of Micro-Patterned Surfaces in Hydrodynamic Lubrication, Trans. ASME 127 (2005) 96-102.

[6] de Krater, A. et al., A Multiscale Method for Modeling Surface Texture Effects, J. Trib, 129 (2007) 221- 230.

[7] Mourier, L. et al., Transient Increase of Film Thickness in Micro-Textured EHL Contacts, Trib. Int. 39 (2006) 1745-1756.

[8] Dumont, M. –L. et al., Surface Feature Effects in Starved Circular EHL Contacts, Trans. ASME 124 (2002) 358-366.

[9] ZSet/ZéBuLoN Version 8.4, Northwest Numerics, Seattle, USA. www.nwnumerics.com

[10] Rodríguez Ripoll, M. et al., Finite Element Analysis of Textured Surfaces under Reciprocating Sliding, Proc. 2nd European Conference on Tribology ECOTRIB 2009, Vol. 2, E. Cuilli, B. Piccigallo, R. Bassani, F. Franek, J. Vižintin, R. Crockett (eds.), (2009), pp. 709-714, ISBN 978-884672426-7.